


Article

Electrocaloric Effect in Different Oriented $\text{BaZr}_{0.15}\text{Ti}_{0.85}\text{O}_3$ Single Crystals

Yun Ou ¹ , Chihou Lei ² and Dongliang Shan ^{3,*}

¹ School of Materials Science and Engineering, Hunan University of Science and Technology, Xiangtan 411201, China

² Department of Aerospace and Mechanical Engineering, Saint Louis University, Saint Louis, MI 63103-1110, USA

³ Key Laboratory of Low Dimensional Materials and Application Technology of Ministry of Education, School of Materials Science and Engineering, Xiangtan University, Xiangtan 411105, China

* Correspondence: dlshan@xtu.edu.cn

Abstract: The electrocaloric effect of ferroelectrics is promising for new solid-state refrigeration. However, the current research on the electrocaloric effect of bulk ferroelectrics mainly focuses on (001) orientation. Thus, we studied the electrocaloric effect of $\text{BaZr}_{0.15}\text{Ti}_{0.85}\text{O}_3$ single crystals with different orientations through the nonlinear thermodynamic approach and entropy analysis. The results show that the dipolar entropy of (111)-oriented $\text{BaZr}_{0.15}\text{Ti}_{0.85}\text{O}_3$ single crystals exhibits a greater change after applying an external electric field, compared with (001)- and (110)-orientations, and the (001)-oriented electrocaloric responses are consistent with experimental observations. The (111)-oriented $\text{BaZr}_{0.15}\text{Ti}_{0.85}\text{O}_3$ single crystals have a more significant electrocaloric response, resulting in a broader work temperature range with a large electrocaloric effect. These insights offer an alternative way to enhance the electrocaloric response of ferroelectric single crystals.

Keywords: electrocaloric effect; barium zirconate titanate; oriented single crystal; broad work temperature range



Citation: Ou, Y.; Lei, C.; Shan, D. Electrocaloric Effect in Different Oriented $\text{BaZr}_{0.15}\text{Ti}_{0.85}\text{O}_3$ Single Crystals. *Materials* **2022**, *15*, 7018. <https://doi.org/10.3390/ma15197018>

Academic Editor: Georgios C. Psarras

Received: 23 August 2022

Accepted: 28 September 2022

Published: 10 October 2022

Publisher's Note: MDPI stays neutral with regard to jurisdictional claims in published maps and institutional affiliations.



Copyright: © 2022 by the authors. Licensee MDPI, Basel, Switzerland. This article is an open access article distributed under the terms and conditions of the Creative Commons Attribution (CC BY) license (<https://creativecommons.org/licenses/by/4.0/>).

1. Introduction

The solid-state refrigeration technology based on the electrocaloric (EC) effect of ferroelectric materials has the characteristics of low noise, high efficiency, and being environmentally friendly [1–8]. It is expected to become a new generation of refrigeration ways leading to potential application prospects [9–11]. Existing studies have shown that the large electrocaloric effect of ferroelectric materials usually occurs near the Curie temperature [12–16]. For example, Mischenko et al. discovered a giant electrocaloric effect of about 12 K under an electric field of 48 MV/m near the Curie temperature in $\text{PbZr}_{0.95}\text{Ti}_{0.05}\text{O}_3$ thin film [12], while Neese et al. discovered a temperature change of 12 K under an electric field of 209 MV/m around the Curie temperature in polymer thin films [17]. However, thin films are limited in practical EC cooling applications due to their smaller thermal mass than bulks [3]. Therefore, the ferroelectric single crystal bulk material has attracted attention. For example, Moya et al. found an electrocaloric effect temperature change of 0.9 K under an electric field of 1.2 MV/m near the Curie temperature in BaTiO_3 single crystal through experiments [13], while Wu et al. found maximum EC strength near the phase boundary of $\text{PbMg}_{1/3}\text{Nb}_{2/3}\text{O}_3$ - PbTiO_3 single crystals by molecular dynamics theory [18].

In recent years, lead-free barium zirconate titanate ($\text{BaZr}_x\text{Ti}_{1-x}\text{O}_3$) has attracted much attention due to its rich phase structure and excellent electrocaloric (EC) properties [19–24]. Direct measurement by Qian et al. indicates that when the change of the electric field is 2.1 MV/m, $\text{BaZr}_{0.2}\text{Ti}_{0.8}\text{O}_3$ ceramics at 38 °C exhibit an EC temperature change of 1.1 °C with a large EC coefficient of around $0.5 \times 10^{-6} \text{ K mV}^{-1}$ [19]. Compared with other ferro-

electric bulk materials, it possesses better EC properties and is an EC material with great application potential [19,20].

Ferroelectric materials with different orientations generate different phase structures, which affect the corresponding material properties [25,26]. Xu et al., using a thermodynamic model, studied the orientation-dependent equilibrium ferroelectric domain structures and dielectric properties of polydomain $\text{PbZr}_{1-x}\text{Ti}_x\text{O}_3$ thin films; the film orientation can deeply influence the phase stability and properties [25]. Li et al. studied the orientation-related electrocaloric effect of $0.7\text{Pb}(\text{Mg}_{1/3}\text{Nb}_{2/3})\text{O}_3$ - 0.3PbTiO_3 (PMN-0.3PT) single crystals, and the (111) oriented PMN-0.3PT single crystals showed a larger electrocaloric response than (110) and (111) orientations near Curie temperature under the electric field of 2.5 kV/cm [27]. The electrocaloric effect is greatly affected by the crystal orientations. However, the current research on $\text{BaZr}_x\text{Ti}_{1-x}\text{O}_3$ and other ferroelectric single crystals mainly focuses on the (001) orientation, while the other orientations, such as the common (110) and (111) orientations, are rarely reported. Therefore, in this letter, the polarization and phase structures of $\text{BaZr}_{0.15}\text{Ti}_{0.85}\text{O}_3$ in (001), (110), and (111) orientations are established by thermodynamic methods. The resulting entropies and the EC temperature changes under different electric fields are further computed. Comparing the EC temperature changes for the three orientations will provide a guideline for enhancing the electrocaloric effect of ferroelectric single crystals.

2. Theoretical Approach

The thermodynamic potential energy of bulk ferroelectrics under stress-free boundary conditions can be expressed as a polynomial of the polarization component P'_l ($l = 1, 2, 3$) and electric field component E'_l [28–35],

$$G'(\mathbf{E}, T) = \alpha_1 (P_1'^2 + P_2'^2 + P_3'^2) + \alpha_{11} (P_1'^4 + P_2'^4 + P_3'^4) + \alpha_{12} (P_1'^2 P_2'^2 + P_2'^2 P_3'^2 + P_1'^2 P_3'^2) + \alpha_{111} (P_1'^6 + P_2'^6 + P_3'^6) + \alpha_{112} [P_1'^2 (P_2'^4 + P_3'^4) + P_2'^2 (P_1'^4 + P_3'^4) + P_3'^2 (P_1'^4 + P_2'^4)] + \alpha_{123} P_1'^2 P_2'^2 P_3'^2 + \alpha_{1111} (P_1'^8 + P_2'^8 + P_3'^8) + \alpha_{1122} (P_1'^4 P_2'^4 + P_2'^4 P_3'^4 + P_1'^4 P_3'^4) + \alpha_{1112} [P_1'^6 (P_2'^2 + P_3'^2) + P_2'^6 (P_1'^2 + P_3'^2) + P_3'^6 (P_1'^2 + P_2'^2)] + \alpha_{1123} (P_1'^4 P_2'^2 P_3'^2 + P_1'^2 P_2'^4 P_3'^2 + P_1'^2 P_2'^2 P_3'^4) - P_1' E'_1 - P_2' E'_2 - P_3' E'_3 \quad (1)$$

where α_1 , α_{ij} , α_{ijk} , and α_{ijkl} are the thermodynamic potential coefficients. Note that all the coefficients are independent of T except α_1 , $\alpha_1 = (T - T_0)/2\epsilon_0 C$, which satisfies the Curie–Weiss law, T_0 is the Curie–Weiss temperature, C is the Curie constant, and ϵ_0 is the permittivity of vacuum.

In this work, three typical orientations, (001), (110), and (111), are considered. The crystallographic axes ($x'_1 x'_2 x'_3$) denote the local coordinate system, where $x'_1 \parallel [100]$, $x'_2 \parallel [010]$, $x'_3 \parallel [001]$. For (001)-, (110)-, and (111)-oriented bulk ferroelectrics, the transformation matrices from local coordinates to global coordinates are expressed as

$$\mathbf{T}_{(001)} = \begin{bmatrix} 1 & 0 & 0 \\ 0 & 1 & 0 \\ 0 & 0 & 1 \end{bmatrix}, \mathbf{T}_{(110)} = \begin{bmatrix} 0 & 0 & 1 \\ \frac{1}{\sqrt{2}} & -\frac{1}{\sqrt{2}} & 0 \\ \frac{1}{\sqrt{2}} & \frac{1}{\sqrt{2}} & 0 \end{bmatrix}, \mathbf{T}_{(111)} = \begin{bmatrix} \frac{1}{\sqrt{2}} & -\frac{1}{\sqrt{2}} & 0 \\ \frac{1}{\sqrt{6}} & -\frac{1}{\sqrt{6}} & -\frac{2}{\sqrt{6}} \\ \frac{1}{\sqrt{3}} & \frac{1}{\sqrt{3}} & \frac{1}{\sqrt{3}} \end{bmatrix} \quad (2)$$

The polarization \mathbf{P}' and the electric field \mathbf{E}' , with respect to the local coordinates, are related to their corresponding global physical quantities, that is, $\mathbf{P}' = \mathbf{T}_{(hkl)}^{-1} \mathbf{P}$ and $\mathbf{E}' = \mathbf{T}_{(hkl)}^{-1} \mathbf{E}$, where \mathbf{P} and \mathbf{E} are the physical quantities with respect to the global coordinates. Notice that the superscript “−1” refers to the matrix inverse, and the subscript (hkl) represents the involved orientation (001), (110), or (111). Thus, the thermodynamic potential energy density of bulk ferroelectric with the (001), (110), and (111) orientations, denoted by $G_{(001)}$, $G_{(110)}$, and $G_{(111)}$, are obtained and presented in the Supplementary Materials, as Equations (S1)–(S3).

To predict the temperature change of the electrocaloric effect of the ferroelectric single crystals with different orientations, the total entropy S_{total} of the ferroelectric crystals is decomposed according to $S_{total}(\mathbf{E}, T) = S_{dip}(\mathbf{E}, T) + S_{latt}(T)$ [36,37], where $S_{dip}(\mathbf{E}, T)$ is the dipolar entropy related to the polarization \mathbf{P} , and $S_{latt}(T)$ is the lattice entropy, which is independent of the applied electric field \mathbf{E} . $S_{latt}(T)$ is assumed to be only correlated to lattice contribution. Due to the adiabatic condition, the total entropy change of the system is zero. The initial state entropy (\mathbf{E}_i, T_i), equal to the final state entropy (\mathbf{E}_f, T_f), leads to

$$S_{latt}(T_f) - S_{latt}(T_i) = -[S_{dip}(\mathbf{E}_f, T_f) - S_{dip}(\mathbf{E}_i, T_i)], \quad (3)$$

Moreover, the change of lattice entropy can be approximated by

$$S_{latt}(T_f) - S_{latt}(T_i) = \int_{T_i}^{T_f} \frac{C_{latt}(T)}{T} dT \approx C_{latt}(T_i) \ln\left(\frac{T_f}{T_i}\right), \quad (4)$$

The approximation is employed in Equation (4) because the variation of $C_{latt}(T)$ on the interval $[T_i, T_f]$ is insignificant. The temperature at the final state T_f can be determined as [36–38]

$$T_f = T_i \exp\left\{-\frac{1}{C_{latt}}[S_{dip}(\mathbf{E}_f, T_f) - S_{dip}(\mathbf{E}_i, T_i)]\right\}. \quad (5)$$

The adiabatic temperature change of the electrocaloric effect can be computed

$$\Delta T = T_f - T_i = T_i \exp\left\{-\frac{1}{C_{latt}}[S_{dip}(\mathbf{E}_f, T_f) - S_{dip}(\mathbf{E}_i, T_i)]\right\} - T_i, \quad (6)$$

where C_{latt} is the lattice heat capacity per unit volume, the subscript i indicates the initial state, and f indicates the final state, revealing that the adiabatic temperature change is connected with the dipolar entropy $S_{dip}(\mathbf{E}, T) = -[\partial G(\mathbf{E}, T)/\partial T]_{\mathbf{E}}$ [38]. Notice that both sides of Equation (6) involve initial temperature T_i and final temperature T_f , and thus are solved numerically by iteration. The polarization can be determined by solving the equilibrium equation $(\partial G/\partial P_i)_{\mathbf{E}} = 0$ [39]. The lattice heat capacity is acquired from available experimental data [40]. For the sake of convenience, the electric field is assumed to be directed along [001] direction in the global coordinate, and the initial electric field \mathbf{E}_i is chosen as zero. The electrocaloric calculations were carried out at temperatures from 20 °C to 140 °C, and the polar axis, favorable to ferroelectricity, is along the (111) direction.

3. Results and Discussion

We first investigated the EC effect in the common (001)-oriented $\text{BaZr}_{0.15}\text{Ti}_{0.85}\text{O}_3$ single crystal, as shown in Figure 1. In the absence of an applied electric field, the polarization is shown in Figure 1a, and its Curie temperature is around 66 °C, which is good agreement with experimental observations [41,42]. The polarizations below the Curie temperature appear as $P_1 = P_2 = P_3 \neq 0$, representing the R phase, and the modulus of the polarization vector increases with the electric field increase, which predicts that the dipoles are more ordered under the electric field, further affecting the dipole entropy. Figure 1b demonstrates the trend of dipolar entropy over a temperature range under different electric fields. The dipolar entropy increases with increasing temperature but decreases with an increasing electric field. A more significant change in the dipolar entropy is observed near the Curie temperature, indicating a larger electrocaloric effect near the Curie temperature.

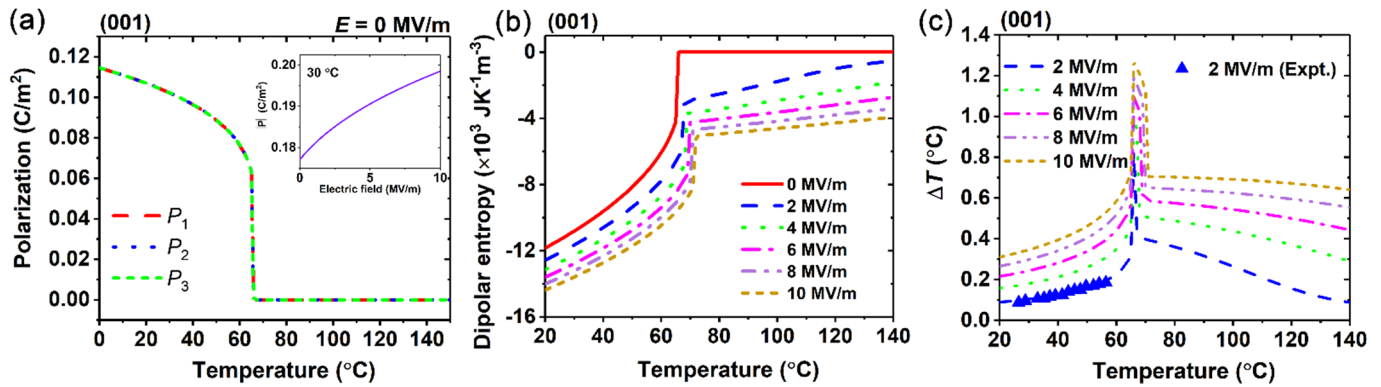


Figure 1. (a) Polarizations of (001)-oriented BaZr_{0.15}Ti_{0.85}O₃ in the absence of an external electric field, and modulus of polarization vector as electric field increases at 30 °C. (b) Dipolar entropy and (c) adiabatic temperature change ΔT under different electric fields as a function of temperature. Experimental data are denoted by blue triangles [21].

The EC temperature change of the (001)-oriented BaZr_{0.15}Ti_{0.85}O₃ single crystal over a range of operating temperature, as shown in Figure 1c, increases until reaching the largest value at the Curie temperature. As the electric field increases, the range of the large EC temperature change becomes wider, due to the increase of the phase transition temperature. For instance, when the electric field change is 2 MV/m, the computational and the experimental data are consistent [21]. Moreover, when the electric field is changed to 10 MV/m, the maximum EC temperature change of the (001)-oriented BaZr_{0.15}Ti_{0.85}O₃ single crystal is 1.27 °C.

The EC effect of the (110)-oriented BaZr_{0.15}Ti_{0.85}O₃ single crystals is illustrated in Figure 2. Below the Curie temperature, the polarizations appear as $P_1 = 0$, $P_2 \neq 0$, and $P_3 \neq 0$, is shown in Figure 2a. Compared with the (001) orientation, the dipolar entropy of the BaZr_{0.15}Ti_{0.85}O₃ single crystals in the (110) orientation experience a greater change after the electric field is applied, as shown in Figure 2b. Thus, the EC temperature change of (110)-oriented crystals can be enhanced from the (001)-oriented crystals. For instance, when the electric field is changed to 10 MV/m, the maximum EC temperature change is 1.64 °C.

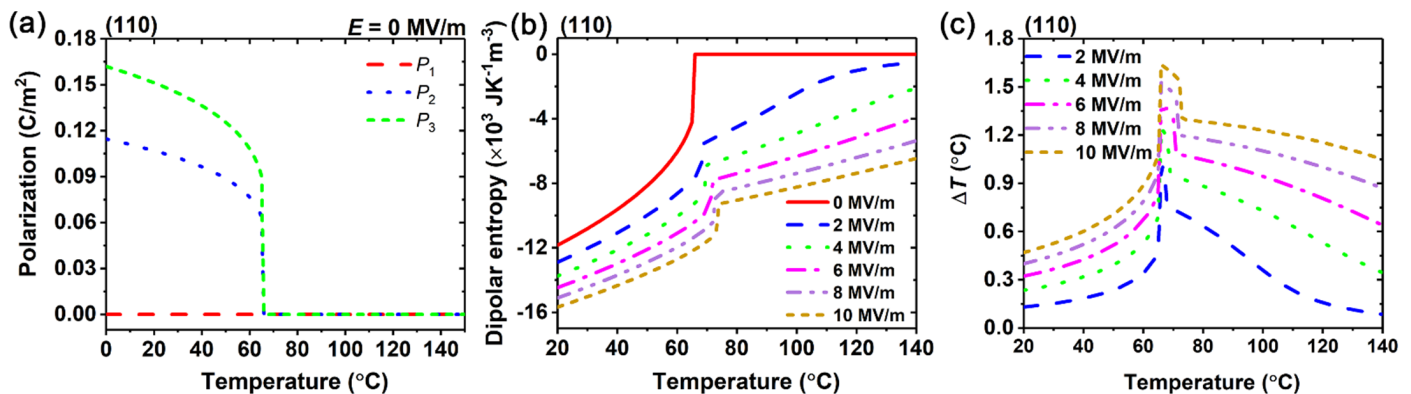


Figure 2. (a) Polarizations of (110)-oriented BaZr_{0.15}Ti_{0.85}O₃ in the absence of an external electric field. (b) Dipolar entropy and (c) adiabatic temperature change ΔT under different electric fields as a function of temperature.

The trends of polarization, entropy, and the electrocaloric effect of (111)-oriented BaZr_{0.15}Ti_{0.85}O₃ single crystals are shown in Figure 3. The trend of polarization below the Curie temperature, with $P_1 = P_2 = 0$ and $P_3 \neq 0$, is shown in Figure 3a. Compared with the dipolar entropies of the (001)- and (110)-oriented BaZr_{0.15}Ti_{0.85}O₃ single crystals, the dipolar entropy of the (111)-oriented BaZr_{0.15}Ti_{0.85}O₃ single crystals under an external electric field varies continuously across the Curie temperature, as shown in Figure 3b.

Thus, the (111)-orientated $\text{BaZr}_{0.15}\text{Ti}_{0.85}\text{O}_3$ single crystals possess a broader temperature range for the large electrocaloric temperature change. For instance, when the electric field is changed at 10 MV/m, the maximum EC temperature change can reach 1.91 °C, while the EC temperature change is larger than 1.5 °C within the temperature range from 66 °C to 128 °C.

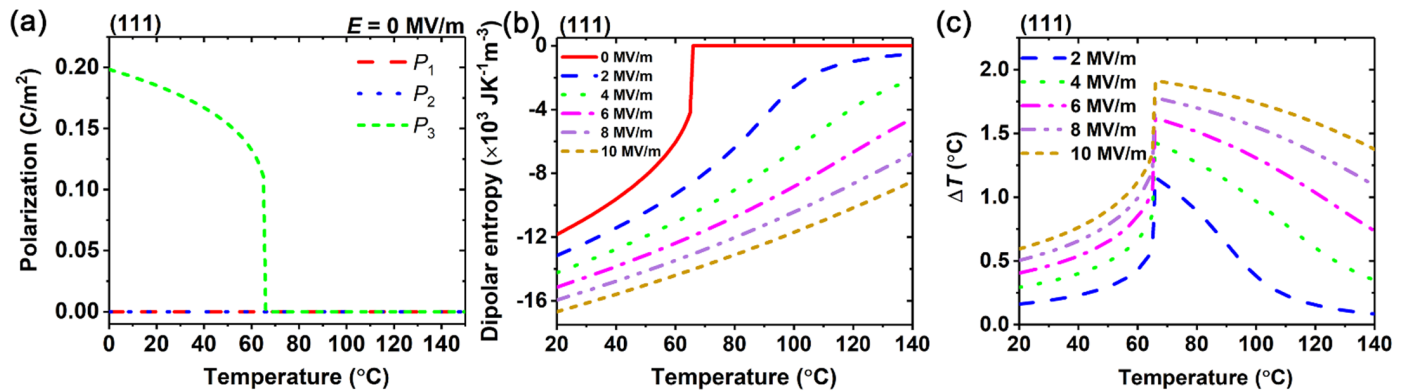


Figure 3. (a) Polarizations of (111)-oriented $\text{BaZr}_{0.15}\text{Ti}_{0.85}\text{O}_3$ in the absence of external electric field. (b) Dipolar entropy and (c) adiabatic temperature change ΔT under different electric fields as a function of temperature.

Finally, we compare the electrocaloric effects of the three orientations, as shown in Figure 4. The EC temperature changes of $\text{BaZr}_{0.15}\text{Ti}_{0.85}\text{O}_3$ single crystals in the three orientations are shown in Figure 4a when the electric field is changed to 10 MV/m. The maximum EC temperature change of the three orientations occurs at 66 °C. The maximum EC temperature change of the (111)-oriented crystals is about 1.5 times that of the (001)-oriented crystal, indicating that the electrocaloric effect becomes significantly enhanced. It can be seen from Figure 4a that the (111)-oriented crystals exhibit a wider temperature range with a large EC temperature response. The trend of the EC temperature changes of $\text{BaZr}_{0.15}\text{Ti}_{0.85}\text{O}_3$ single crystals with the three orientations at 25 °C over the electric field are shown in Figure 4b. With the increase of the electric field, the EC temperature changes of the three orientations all increase, where those of (110)- and (111)-orientations are significantly higher than those of the (001)-orientation. The EC temperature change of the (111)-orientation is about 1.9 times that of the (001)-orientation at 12 MV/m. Due to the external applied electric field direction being the same as the polarization direction in (111)-oriented $\text{BaZr}_{0.15}\text{Ti}_{0.85}\text{O}_3$ single crystals, the polarization of (111)-oriented $\text{BaZr}_{0.15}\text{Ti}_{0.85}\text{O}_3$ single crystals is easier to change compared with (001)- and (110)-orientations, as the more polarization change lead to more entropy change, resulting in a larger electrocaloric effect temperature change in (111)-oriented $\text{BaZr}_{0.15}\text{Ti}_{0.85}\text{O}_3$ single crystals. This suggests that the EC performance of the ferroelectric single crystals can be enhanced by choosing suitable orientations.

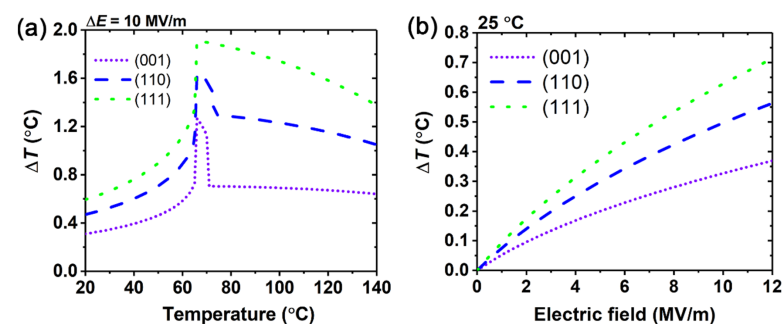


Figure 4. Comparison of electrocaloric responses in $\text{BaZr}_{0.15}\text{Ti}_{0.85}\text{O}_3$ single crystals with different orientations. (a) As a function of temperature under an electric field change $\Delta E = 10$ MV/m; (b) As a function of an electric field at 25 °C.

4. Conclusions

In conclusion, the polarization, the dipole entropy, and the electrocaloric temperature changes of (001)-, (110)-, and (111)-oriented $\text{BaZr}_{0.15}\text{Ti}_{0.85}\text{O}_3$ single crystals were studied by developing the thermodynamic theory. The predicted results are in good agreement with the experiments. Compared to the (001)- and (110)-orientations, the polarization of the (111)-oriented $\text{BaZr}_{0.15}\text{Ti}_{0.85}\text{O}_3$ single crystals is greatly improved, where the dipolar entropy further increases after the electric field is applied. Thus, (111)-oriented $\text{BaZr}_{0.15}\text{Ti}_{0.85}\text{O}_3$ single crystals exhibit excellent electrocaloric performance with a broader work temperature range of large EC temperature changes, which provides insight into enhancing the EC properties of ferroelectric single crystals in general.

Supplementary Materials: The following supporting information can be downloaded at: <https://www.mdpi.com/article/10.3390/ma15197018/s1>, Equation (S1): The thermodynamic potential energy density of the (001)-oriented bulk ferroelectric, Equation (S2): The thermodynamic potential energy density of the (110)-oriented bulk ferroelectric, Equation (S3): The thermodynamic potential energy density of the (111)-oriented bulk ferroelectric.

Author Contributions: Y.O.: Conceptualization, theoretical calculations, writing the original draft. C.L.: Analysis of data, review, and editing. D.S.: Conceptualization, methodology, review, and editing, interpretation of analyzed data. All authors have read and agreed to the published version of the manuscript.

Funding: This work was partially supported by the National Natural Science Foundation of China (11702092, 12102378), and the project was supported by the Hunan Provincial Natural Science Foundation of China (2020JJ5182). Lei acknowledges the startup fund supported jointly by the Dean of Parks College and the Provost of Saint Louis University.

Institutional Review Board Statement: Not applicable.

Informed Consent Statement: Not applicable.

Data Availability Statement: Not applicable.

Conflicts of Interest: The authors declare no conflict of interest.

References

- Wang, Y.; Zhang, Z.; Usui, T.; Benedict, M.; Hirose, S.; Lee, J.; Kalb, J.; Schwartz, D. A high-performance solid-state electrocaloric cooling system. *Science* **2020**, *370*, 129–133. [[CrossRef](#)] [[PubMed](#)]
- Qian, X.S.; Han, D.L.; Zheng, L.R.; Chen, J.; Tyagi, M.; Li, Q.; Du, F.H.; Zheng, S.; Huang, X.Y.; Zhang, S.H.; et al. High-entropy polymer produces a giant electrocaloric effect at low fields. *Nature* **2021**, *600*, 664–669. [[CrossRef](#)] [[PubMed](#)]
- Shi, J.Y.; Han, D.L.; Li, Z.C.; Yang, L.; Lu, S.G.; Zhong, Z.F.; Chen, J.P.; Zhang, Q.M.; Qian, X.S. Electrocaloric cooling materials and devices for zero-global-warming-potential, high-efficiency refrigeration. *Joule* **2019**, *3*, 1200–1225. [[CrossRef](#)]
- Li, X.Y.; Lu, S.G.; Chen, X.Z.; Gu, H.M.; Qian, X.S.; Zhang, Q.M. Pyroelectric and electrocaloric materials. *J. Mater. Chem. C* **2013**, *1*, 23–37. [[CrossRef](#)]
- Scott, J.F. Electrocaloric materials. *Annu. Rev. Mater. Res.* **2011**, *41*, 229–240. [[CrossRef](#)]
- Shi, J.; Zhu, R.F.; Liu, X.; Fang, B.J.; Yuan, N.Y.; Ding, J.N.; Luo, H.S. Large electrocaloric effect in lead-free $(\text{Ba}_{0.85}\text{Ca}_{0.15})(\text{Zr}_{0.1}\text{Ti}_{0.9})\text{O}_3$ ceramics prepared via citrate route. *Materials* **2017**, *10*, 1093. [[CrossRef](#)] [[PubMed](#)]
- Asbani, B.; Gagou, Y.; Ben Moumen, S.; Dellis, J.-L.; Lahmar, A.; Amjoud, M.B.; Mezzane, D.; El Marssi, M.; Rozic, B.; Kutnjak, Z. Large electrocaloric responsivity and energy storage response in the lead-free $\text{Ba}(\text{Ge}_x\text{Ti}_{1-x})\text{O}_3$ ceramics. *Materials* **2022**, *15*, 5227. [[CrossRef](#)]
- Hou, X.; Li, H.Y.; Shimada, T.; Kitamura, T.; Wang, J. Effect of geometric configuration on the electrocaloric properties of nanoscale ferroelectric materials. *J. Appl. Phys.* **2018**, *123*, 124103. [[CrossRef](#)]
- Correia, T.; Zhang, Q. *Electrocaloric Materials: New Generation of Coolers*; Springer: Berlin, Germany, 2014.
- Moya, X.; Mathur, N.D. Caloric materials for cooling and heating. *Science* **2020**, *370*, 797–803. [[CrossRef](#)]
- Meng, Y.; Zhang, Z.Y.; Wu, H.X.; Wu, R.Y.; Wu, J.H.; Wang, H.L.; Pei, Q.B. A cascade electrocaloric cooling device for large temperature lift. *Nat. Energy* **2020**, *5*, 996–1002. [[CrossRef](#)]
- Mischenko, A.S.; Zhang, Q.; Scott, J.F.; Whatmore, R.W.; Mathur, N.D. Giant electrocaloric effect in thin-film $\text{PbZr}_{0.95}\text{Ti}_{0.05}\text{O}_3$. *Science* **2006**, *311*, 1270–1271. [[CrossRef](#)] [[PubMed](#)]
- Moya, X.; Stern-Taulats, E.; Crossley, S.; Gonzalez-Alonso, D.; Kar-Narayan, S.; Planes, A.; Manosa, L.; Mathur, N.D. Giant electrocaloric strength in single-crystal BaTiO_3 . *Adv. Mater.* **2013**, *25*, 1360–1365. [[CrossRef](#)] [[PubMed](#)]

14. Shan, D.L.; Pan, K.; Lei, C.H.; Peng, J.L.; He, N.B.; Pan, J.Y.; Jin, H.Y.; Liu, Y.Y. Large electrocaloric response over a broad temperature range near room temperature in $\text{Ba}_x\text{Sr}_{1-x}\text{TiO}_3$ single crystals. *J. Appl. Phys.* **2019**, *126*, 204103. [\[CrossRef\]](#)
15. Moya, X.; Kar-Narayan, S.; Mathur, N.D. Caloric materials near ferroic phase transitions. *Nat. Mater.* **2014**, *13*, 439–450. [\[CrossRef\]](#)
16. Bai, G.; Qin, X.S.; Xie, Q.Y.; Gao, C.F. Electric-field-induced phase transition and electrocaloric effect in PZT near morphotropic phase boundary. *Phys. B* **2019**, *560*, 208–214. [\[CrossRef\]](#)
17. Neese, B.; Chu, B.J.; Lu, S.G.; Wang, Y.; Furman, E.; Zhang, Q.M. Large electrocaloric effect in ferroelectric polymers near room temperature. *Science* **2008**, *321*, 821–823. [\[CrossRef\]](#)
18. Wu, H.H.; Cohen, R.E. Electric-field-induced phase transition and electrocaloric effect in PMN-PT. *Phys. Rev. B* **2017**, *96*, 054116. [\[CrossRef\]](#)
19. Qian, X.S.; Ye, H.J.; Zhang, Y.T.; Gu, H.M.; Li, X.Y.; Randall, C.A.; Zhang, Q.M. Giant electrocaloric response over a broad temperature range in modified BaTiO_3 ceramics. *Adv. Funct. Mater.* **2014**, *24*, 1300–1305. [\[CrossRef\]](#)
20. Qian, J.F.; Hu, P.H.; Liu, C.; Jiang, J.Y.; Dan, Z.K.; Ma, J.; Lin, Y.H.; Nan, C.W.; Shen, Y. High electrocaloric cooling power of relaxor ferroelectric $\text{BaZr}_x\text{Ti}_{1-x}\text{O}_3$ ceramics within broad temperature range. *Sci. Bull.* **2018**, *63*, 356–361. [\[CrossRef\]](#)
21. Jian, X.D.; Lu, B.; Li, D.D.; Yao, Y.B.; Tao, T.; Liang, B.; Guo, J.H.; Zeng, Y.J.; Chen, J.L.; Lu, S.G. Direct measurement of large electrocaloric effect in $\text{Ba}(\text{Zr}_x\text{Ti}_{1-x})\text{O}_3$ ceramics. *ACS Appl. Mater. Inter.* **2018**, *10*, 4801–4807. [\[CrossRef\]](#)
22. Shan, D.L.; Cai, Y.C.; Lei, C.H.; Peng, J.L.; He, N.B.; Pan, K.; Liu, Y.Y.; Li, J.Y. Electric-field-driven coexistence of positive and negative electrocaloric effects near room temperature for high-efficiency two-stage cooling. *Appl. Phys. Lett.* **2021**, *118*, 122905. [\[CrossRef\]](#)
23. Peng, J.L.; Shan, D.L.; Liu, Y.Y.; Pan, K.; Lei, C.H.; He, N.B.; Zhang, Z.Y.; Yang, Q. A thermodynamic potential for barium zirconate titanate solid solutions. *npj Comput. Mater.* **2018**, *4*, 66. [\[CrossRef\]](#)
24. Co, K.; Khassaf, H.; Alpay, S.P. Electrocaloric and pyroelectric properties of barium zirconate titanate. *J. Appl. Phys.* **2020**, *127*, 174102. [\[CrossRef\]](#)
25. Xu, R.J.; Zhang, J.L.; Chen, Z.H.; Martin, L.W. Orientation-dependent structural phase diagrams and dielectric properties of $\text{PbZr}_{1-x}\text{Ti}_x\text{O}_3$ polydomain thin films. *Phys. Rev. B* **2015**, *91*, 144106. [\[CrossRef\]](#)
26. Xu, R.J.; Liu, S.; Grinberg, I.; Karthik, J.; Damodaran, A.R.; Rappe, A.M.; Martin, L.W. Ferroelectric polarization reversal via successive ferroelastic transitions. *Nat. Mater.* **2015**, *14*, 79–86. [\[CrossRef\]](#)
27. Li, J.T.; Yin, R.W.; Su, X.P.; Wu, H.H.; Li, J.J.; Qin, S.Q.; Sun, S.D.; Chen, J.; Su, Y.J.; Qiao, L.J.; et al. Complex phase transitions and associated electrocaloric effects in different oriented PMN-30PT single crystals under multi-fields of electric field and temperature. *Acta Mater.* **2020**, *182*, 250–256. [\[CrossRef\]](#)
28. Liu, Y.Y.; Zhu, Z.X.; Li, J.F.; Li, J.Y. Misfit strain modulated phase structures of epitaxial $\text{Pb}(\text{Zr}_{1-x}\text{Ti}_x)\text{O}_3$ thin films: The effect of substrate and film thickness. *Mech. Mater.* **2010**, *42*, 816–826. [\[CrossRef\]](#)
29. Liu, Y.Y.; Li, J.Y. Shear-driven morphotropic phase boundary in epitaxial ferroelectric thin films. *Phys. Rev. B* **2011**, *84*, 132104. [\[CrossRef\]](#)
30. Liu, Y.Y.; Yang, L.; Li, J.Y. Strain-engineered orthorhombic-rhombohedral phase boundary in epitaxial bismuth ferrite films. *J. Appl. Phys.* **2013**, *113*, 183524. [\[CrossRef\]](#)
31. Li, Y.L.; Cross, L.E.; Chen, L.Q. A phenomenological thermodynamic potential for BaTiO_3 single crystals. *J. Appl. Phys.* **2005**, *98*, 064101. [\[CrossRef\]](#)
32. Liu, Y.Y.; Vasudevan, R.K.; Pan, K.; Xie, S.H.; Liang, W.I.; Kumar, A.; Jesse, S.; Chen, Y.C.; Chu, Y.H.; Nagarajan, V.; et al. Controlling magnetoelectric coupling by nanoscale phase transformation in strain engineered bismuth ferrite. *Nanoscale* **2012**, *4*, 3175–3183. [\[CrossRef\]](#) [\[PubMed\]](#)
33. Liu, N.; Su, Y.; Weng, G.J. A phase-field study on the hysteresis behaviors and domain patterns of nanocrystalline ferroelectric polycrystals. *J. Appl. Phys.* **2013**, *113*, 204106. [\[CrossRef\]](#)
34. Pertsev, N.A.; Zembilgotov, A.G.; Tagantsev, A.K. Effect of mechanical boundary conditions on phase diagrams of epitaxial ferroelectric thin films. *Phys. Rev. Lett.* **1998**, *80*, 1988–1991. [\[CrossRef\]](#)
35. Liu, Y.Y.; Li, J.Y. Seeing is believing: Negative capacitance captured at both nano- and macro-scales. *Sci. Bull.* **2019**, *64*, 361–363. [\[CrossRef\]](#)
36. Pirc, R.; Kutnjak, Z.; Blinc, R.; Zhang, Q.M. Electrocaloric effect in relaxor ferroelectrics. *J. Appl. Phys.* **2011**, *110*, 074113. [\[CrossRef\]](#)
37. Liu, Y.; Scott, J.F.; Dkhil, B. Direct and indirect measurements on electrocaloric effect: Recent developments and perspectives. *Appl. Phys. Rev.* **2016**, *3*, 031102. [\[CrossRef\]](#)
38. Shan, D.L.; Lei, C.H.; Cai, Y.C.; Pan, K.; Liu, Y.Y. Mechanical control of electrocaloric response in epitaxial ferroelectric thin films. *Int. J. Solids Struct.* **2021**, *216*, 59–67. [\[CrossRef\]](#)
39. Peng, J.L.; Li, Q.; Shan, D.L.; Pan, K.; Yu, G.S.; Liu, Y.Y. Phenomenological thermodynamic potentials for bulk and thin-film $\text{Ba}(\text{Zr}_{0.08}\text{Ti}_{0.92})\text{O}_3$ single crystals. *J. Appl. Phys.* **2016**, *119*, 204103. [\[CrossRef\]](#)
40. Jian, X.D.; Lu, B.; Li, D.D.; Yao, Y.B.; Tao, T.; Liang, B.; Lu, S.G. Large electrocaloric effect in lead-free $\text{Ba}(\text{Zr}_x\text{Ti}_{1-x})\text{O}_3$ thick film ceramics. *J. Alloys Compd.* **2018**, *742*, 165–171. [\[CrossRef\]](#)
41. Mahesh, M.L.V.; Prasad, V.V.B.; James, A.R. Enhanced dielectric and ferroelectric properties of lead-free $\text{Ba}(\text{Zr}_{0.15}\text{Ti}_{0.85})\text{O}_3$ ceramics compacted by cold isostatic pressing. *J. Alloys Compd.* **2014**, *611*, 43–49. [\[CrossRef\]](#)
42. Yu, Z.; Guo, R.Y.; Bhalla, A.S. Dielectric behavior of $\text{Ba}(\text{Ti}_{1-x}\text{Zr}_x)\text{O}_3$ single crystals. *J. Appl. Phys.* **2000**, *88*, 410–415. [\[CrossRef\]](#)